UNIVERSITY OF CAMBRIDGE
Department of Architecture

Methodologies for assessing urban microclimates

Kanchane Gunawardena M.Phil(*Cantab*) Ph.D(*Cantab*)

The Martin Centre for Architectural and Urban Studies
Department of Architecture University of Cambridge, 1-5 Scroope Terrace, Cambridge, CB2 1PX, UK

1.0 Introduction

The environmental thermal loading on urban buildings is governed by its climate. It has long been recognised that cities exhibit distinct climates, and are typically warmer than surrounding rural areas to describe the influence of the urban heat island (UHI) effect. This distinctiveness must be accounted for when assessing urban energy interactions, with site-specific loading assessments requiring the procurement of data that defines the local microclimate, either from monitoring campaigns, or calculated from governing variables. This paper reviews the state-of-the-art of the latter simulation approaches. An abridged version of this review is also represented by Gunawardena (2021).

2.0 Characterising urban climates

The data from standard weather station compiled or generated weather files do not always correspond to an urban area under study, nor account for the site-specific influence of the heat island (Sailor 2011). Microclimate variations resulting from distinct morphological features and localised heat sinks and sources such as green spaces and waterbodies are not typically captured by the resolution of these weather files. This shortcoming may be resolved by sourcing site-specific measurement data from direct techniques to compile localised weather profiles (i.e., using thermocouples, thermistors, etc.). For these measurements to be representative however, the data would require longitudinal measurement to account for the spatial and temporal variation in heat island influence (Oke 1987). This requirement would favour data collection approaches with dense networks of fixed monitoring stations, as opposed to mobile traverse monitoring that offers only cross-sectional data. There is however no general scheme or commonly accepted standard practice to direct such measurement practices currently in place for most cities (Grimmond *et al.* 2010b; Gunawardena 2018). This means that proposed studies would have to setup their own procedures and infrastructure to gather data. While measurement-based studies notably exist (e.g., Hidalgo *et al.* 2008; Kolokotroni *et al.* 2007; Pigeon *et al.* 2006), the infrastructural expenditure required to achieve similar regimes of data collection is unlikely to be feasible or available for typical assessments with limited resources (Oxizidis *et al.* 2008). Data collected from private networks and contributions from private enthusiasts may be considered as an alternative. This data however is likely to be unreliable, with limited or incompatible parameters collected, and datasets typically demonstrating gaps that may require resource intensive interpolation methods to complete.

$$UHI\ \Delta T_{max} = 7.54 + 3.97\ ln(H\ /\ W) \qquad \textit{Equation 1}$$

Where,

H	Canyon height [m]
W	Canyon width [m]

As an alternative to acquiring measured data, temperatures including heat island influence may be estimated from representative historical data and identified statistical relationships. Typical statistical approaches offer simple linear or multiple regression models to calculate heat island intensities as a function of relevant site-specific variables (Grimmond *et al.* 2010b). Oke (1981) for example, used strong correlations between canyon geometry and maximum heat island intensity data for mid-latitude cities to propose a regression model that estimates the maximum nocturnal heat island intensity experienced within an urban canyon, under ideal anticyclonic weather conditions (Equation 1). The static maximum value presented however is not relatable to real-world heat island intensities experienced, where Oke's own field observations had demonstrated significant diurnal and seasonal dynamic variation. To address this shortcoming, Crawley (2007) considered additional empirical data and sinusoidal profile diagrams from Oke (1982), to present an algorithmic approach to account for dynamic heat island temperature variations by transforming standard weather file dry-bulb temperatures and recalculating the humidity ratio. A key disadvantage of this and similar statistical and mathematical morphing approaches is that they are based on city-specific historical data, and overlook the complex physical interactions that heat island research has repeatedly identified as significant in determining site-specific urban microclimate conditions (Grimmond *et al.* 2010b).

To include the relevance of physical interactions, hybrid approaches have been used to reconcile historical data relationships with physical energy balances. An example of such a hybrid approach is presented by the 'London Site Specific Air Temperature' (LSSAT) model, which utilised machine-learning (Kolokotroni *et al.* 2009). This model was developed using a back-propagation Artificial Neural Network (ANN), based on hourly air temperature readings from 77 sites (data collected as part of the 'Local Urban Climate Model and its Application to the Intelligent Design of Cities' or LUCID project), hourly weather data from Heathrow, and supported by the six site-specific physical parameters of aspect ratio, plan density ratio, fabric density ratio, green density ratio, thermal mass, and surface albedo (parameters acknowledged by Kolokotroni & Giridharan, 2008). The resulting trained ANN model is able to estimate air temperatures at a specific site and time within the heat island, based on data from a single weather station and historic measured air temperatures (Kolokotroni *et al.* 2010). This and similar ANN-based hybrid approaches are claimed to provide improved heat island intensity predictions. For example, a comparison study between a multiple linear regression model and an ANN model found that the latter was able to provide improved predictions by up to 6.5% (Kim & Baik 2002). Another hybrid methodology is presented by volume-averaged energy balance approaches, exemplified by the Objective Hysteresis Model. This model parameterises the historical relationship between net radiation and heat storage, with the residual balance partitioned as sensible and latent flux (Grimmond *et al.* 1991). Both these hybrid approaches notably require significant empirical data availability. This in turn highlights their shortcoming, with such data requirements typically restricted by availability and/or quality (resolution and frequency) for the city of interest. Furthermore, model coefficients reliant on statistical determination questions their applicability to cities from different climates zones.

Physical modelling in climatological studies involves the resolution of a volumetric energy balance that encompasses the immediate subsurface, built environment morphology, and the atmospheric domain. The simplest representation of this is presented by 'slab models', where the built environment within the domain is represented as a singular averaged volume. This significant simplification means that they still rely on observational inputs, while heat storage and advection terms are typically determined as a residual (e.g., Oke, 1987). The averaging also means that these models offer little understanding of the interactions between built environment components. The dependence of morphological features such as the differences in contextual surface temperatures are therefore not included. To address this shortcoming, street canyon energy balances have been considered as the generic and simplified representation of the urban microscale, with either single-layer or multilayer models. Single-layer models use a simplified geometric representation with averaged height, width, and orientation for a canyon that interacts with only a single atmospheric layer above the highest roof level (e.g., the Town Energy Balance or TEB model presented by Masson, 2000). These calculate shading and multiple reflection influences on the surface energy balances of walls, roofs, and the road to present a simplified representation of morphological influences. The averaging of temperature, humidity, and wind velocity however means that the canyon climate is assumed to have uniform vertical structures for these variables, which is not representative of real-world conditions. To address this complexity, several atmospheric levels are coupled in multilayer models (e.g., Martilli *et al.,* 2002). This enables them to represent shading from local obstructions and resultant differential heating of surfaces, as well as rudimentary turbulent profiles within the canyon and roughness sublayer. The increased number of layers considered increases accuracy, although at substantial computational expense. To minimise this cost Martilli *et al.* (2002) for example, limited the vertical resolution to 10 m for the first 50 m of the canyon elevation.

To understand surface interactions in the roughness sublayer, atmospheric fluid flow can be modelled using empirical, analytical, or numerical methods. Empirical modelling typically involves wind-tunnel or water-tank testing of a scaled reproduction of a site, with similarity criteria satisfied to account for the scale difference (Grimmond *et al.* 2010b). The complexities of scaling down real-world conditions mean that only stable stratified flow over regular terrain could be expected to present reasonable approximation. Even in such instances, it is not possible to convincingly replicate effects such as buoyancy-driven flow. The opportunity for approximating heat island influence within complex urban arrangements is therefore limited with an empirical modelling approach. Analytical modelling overcomes this by using fundamental analysis methods to solve the problem entirely or as subsets of equations relating to controlled instances. An exact solution is sought for the system of equations that includes the conservation relationships of mass, momentum, and energy by removing their nonlinearities through simplification. The exact nature of the analytical solutions derived from these models provide some approximation of the physical processes involved, with the advantage of eliminating uncertainty associated with computational errors. This simplification however means that complex nonlinearities of the governing flow equations of real-world atmospheric phenomena are not well-expressed by such analytical models (Jacobson 2005). Numerical modelling discretise the governing nonlinear differential equations in space and time, and solve them by using either a finite difference (FDM), finite element (FEM), or finite volume (FVM) approach; the latter being common in computational fluid dynamics (CFD) analyses (Chung 2002). Most such approaches use empirical models tested in wind-tunnels to benchmark numerical codes, and when solved with appropriate boundary conditions, temperature, pressure, and velocity

profiles can be plotted onto a predefined numerical grid to offer reasonable representations of atmospheric flow (Chung 2002). The principal disadvantage of such CFD approaches is their high computational cost, which limits their application in terms of the spatial domain (resolution grid) and temporal requirements (dynamic simulation). Computational fluid dynamics is therefore typically applied to the smallest representative condition of interest (spatially and temporally), with the microscale street canyon often selected for urban assessments (Erell & Williamson 2006). In certain approaches, the outputs from such canyon models have been used to develop parametrisation schemes that are then used in higher-scale models to represent microscale processes, while few have even sought to nest CFD code directly into higher-scale models (Grimmond *et al.* 2010b). In summary, physically-based fluid flow approaches to modelling urban climate interactions may include empirical, analytical, or numerical means described above either exclusively, or as an algorithmic approach to address the scaling challenges of such conditions (Grimmond *et al.* 2010b; Jacobson 2005).

Governing equations of atmospheric flow:

Mass

$$\frac{\partial \rho}{\partial t} + \nabla\,(\rho \vec{u}) = 0 \qquad \textit{Equation 2}$$

Momentum

$$\rho\left(\frac{\partial \vec{u}}{\partial t} + \vec{u}\ \nabla \vec{u}\right) = -\nabla p + \mu \nabla^2\,\vec{u} + \vec{f} \qquad \textit{Equation 3}$$

Energy

$$\rho\left(\frac{\partial c_p T}{\partial t} + \vec{u}\ \nabla T\right) = \mu \nabla^2\, T + Q_T \qquad \textit{Equation 4}$$

Where,

ρ	Density [kg·m^{-3}]	Q_T	Source term for the energy equation [W·m^{-2}]
μ	Dynamic viscosity [Pa·s]	c_p	Specific heat capacity of air [J·kg^{-1}·K^{-1}]
$\vec{u}$	Instantaneous velocity vector [m·s^{-1}]	T	Temperature [K]
$\vec{f}$	Momentum source [kg·m·s^{-1}]	t	Time [s]
p	Pressure [Pa]		

The principal challenge of physically-based approximation of the urban climate relates to how spatial and temporal scales are considered (Grimmond *et al.* 2010b). The definition of scale depends on the agenda and resolution to which modelling approaches target their outcomes (Grimmond *et al.* 2010a; Jacobson 2005; Oke 1987). Most approaches in the past as noted earlier have worked to climatological scaling, ranging from large-scale/macroscale/synoptic-scale, mesoscale, local-scale, to microscale resolutions, while recent approaches have expanded further to include regional (100-200 km), city (10-20 km), neighbourhood (1-2 km), and street canyon (<100 m) resolutions. Depending on which resolution is considered, modelling approaches may determine the processes that need to be explicitly resolved, the ones that can be implicitly addressed through parametrisation, and finally if any could be completely disregarded through assumptions (Jacobson 2005; Oke 1987). Climatologists for example may consider global-to-mesoscale effects as their concentration, while microscale processes may be disregarded based on the assumption that such detailed processes are inconsequential to their scale of interest. In contrast, a building modelling approach might consider only the immediate microscale processes sensitive to their measures of interest, with large-scale processes inputted as parametrised boundary conditions rather than being explicitly resolved.

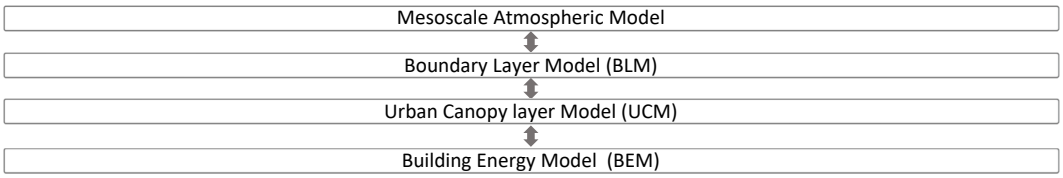

Figure 1. Generic multiscale coupling structure.

A systematic approach to considering an urban climate requires an integrated methodology that resolves all processes across all spatial and temporal scales to provide a realistic approximation. Developing a single model to resolve complexities across all such scale distinctions is not achievable with the computational power available in the present-day. Even if this were to be realised with the use of supercomputers, such models would have little opportunity for common application. Researchers examining urban climate problems have therefore focused on developing 'frameworks', utilising 'parameterisation', 'nesting', or 'multiscale coupling' (Grimmond *et al.* 2010a; Jacobson 2005). Parameterisation refers to the methodology of exchanging processes that are either of finer resolution or too complex to be physically represented and explicitly resolved in the model, with a simplified process. Nesting involves the embedding of a detailed inner model within a coarser resolution outer model, in either one-way or two-way interactions. The advantage of this is that it makes possible to account for microscale features deemed sensitive to a measure of interest, without needing the computational power of using a higher resolution over the entire model domain; a feature that is significant for numerical exercises (Jacobson 2005). With multiscale coupling, the sub-models remain discrete yet interact with one another in one-way, two-way, or multiple exchanges across the scales (Figure 1). Keeping sub-models discrete in such frameworks favours the integration and utilisation of multiple approaches, with empirical, analytical, and numerical methods available to solve problems relating to discrete spatial and temporal scales (Jacobson 2005).

Recent models considering microscale processes have scaled-down their resolution to include buildings in their coupled frameworks. The approach of coupling a building energy model (BEM) with higher-scale canopy and urban boundary layer models provide the benefit of including reasonably realistic representations of buildings and their heating, ventilation, and air conditioning (HVAC) systems to resolve interactions with the urban climate. Kikegawa *et al.* (2003) presented one of the earliest examples that coupled a mesoscale atmospheric model and an urban canopy layer model (UCM) with a simplified building energy sub-model. A later study addressed the shortcomings of this model by integrating a more detailed bespoke building energy model to a Town Energy Balance canyon model (TEB by Masson, 2000), which allowed for substantial complexity in evaluating HVAC systems, while also providing plug-ins for the assessment of passive solutions such as shading and natural ventilation (Bueno *et al.* 2012a). This BEM-TEB coupled approach is capable of estimating building energy consumption at the city-scale (~10 km), with a neighbourhood resolution of ~100 m, while also simulating the energy-use feedback to the urban climate (anthropogenic emissions) (Bueno *et al.* 2012b). A continuation analysis of the results of this BEM-TEB application, revealed a building's surrounding surface temperatures to be critical in resolving the longwave radiation balance of its walls, and consequently in the evaluation of its cooling demand. The advantage offered by the TEB model integration is that such surface radiation balances are explicitly resolved, while in an isolated building energy model simulation (e.g., EnergyPlus by Crawley *et al.,* 2001), these temperatures are approximated to air temperatures (Pigeon *et al.* 2014).

Table 1. Preceding studies that have characterised urban climates through modelling methods.

Previous models	Description	Reference
Cluster Thermal Time Constant (CTTC) model Empirical analytical model	Calculates urban air temperatures from rural weather data by applying simple analytical expressions that account for storage and heat release from the built environment (represented as a lumped body characterised by a sky-view factor and the CTTC parameter that measures thermal inertia). Empirical parameters require calibration at the site of interest (hot-arid climate site reviewed), while it disregards mesoscale heat island influence.	Swaid & Hoffman (1990)
Canyon Air Temperature (CAT) model Empirical analytical model	Developed from the CTTC model, it transforms rural weather station data based on the Local-Scale Urban Meteorological Parameterisation Scheme (LUMPS) from Grimmond & Oke (2002), to provide site-specific air temperatures. It is limited to parameters monitored at stations and canyon morphologies. Review is also required on the applicability of case study (Adelaide, Australia) derived empirical calibration factors.	Erell & Williamson (2006)
Kikegawa *et al.* (2003) Numerical simulation framework	Framework composed of a mesoscale meteorological model with a one-way connection to a bespoke one-dimensional urban canopy layer model, coupled with a bespoke building energy model. Its use is limited to summertime reviews.	Kikegawa *et al.* (2003), evaluated by Kondo & Kikegawa (2003).
Oxizidis *et al.* (2008) Downscaling with mixed method framework	Downscaling of non-hydrostatic mesoscale model simulations with microscale CFD and statistical models, and EnergyPlus simulations to generate synthetic urban weather files.	Oxizidis *et al.* (2008).
EnergyPlus-TEB model Energy balance based coupled framework	Coupled scheme between a detailed building energy model (EnergyPlus) and an urban canopy layer model (TEB). The iterative framework makes it unsuitable for coupling with mesoscale atmospheric models.	Bueno *et al.* (2011).
Resistance-capacitance network model Numerical framework	Urban canopy layer and building energy model coupling, based on a thermal network of constant resistances and capacitances. Fundamental physical relations only, and simplified for computational efficiency.	Bueno *et al.* (2012a).
BEM-TEB model Energy balance based coupled framework	Coupled scheme between a bespoke building energy model and the TEB canopy layer model. The building energy model includes modules for active and passive building systems.	Bueno *et al.* (2012b), evaluated by Pigeon *et al.* (2014).
ENVI-met Microscale numerical model	Non-hydrostatic model that simulates surface-plant-air interactions within the canopy layer. Typical horizontal resolution of 0.5-10 m, and timeframe of 24-48 hrs with a 10 s time-step, which allows for microscale interactions between discrete buildings, surrounding surfaces, and plants.	Bruse (2004), version (4.0) evaluated by Yang *et al.* (2013).

2.1 Exemplar framework: Urban Weather Generator (UWG)

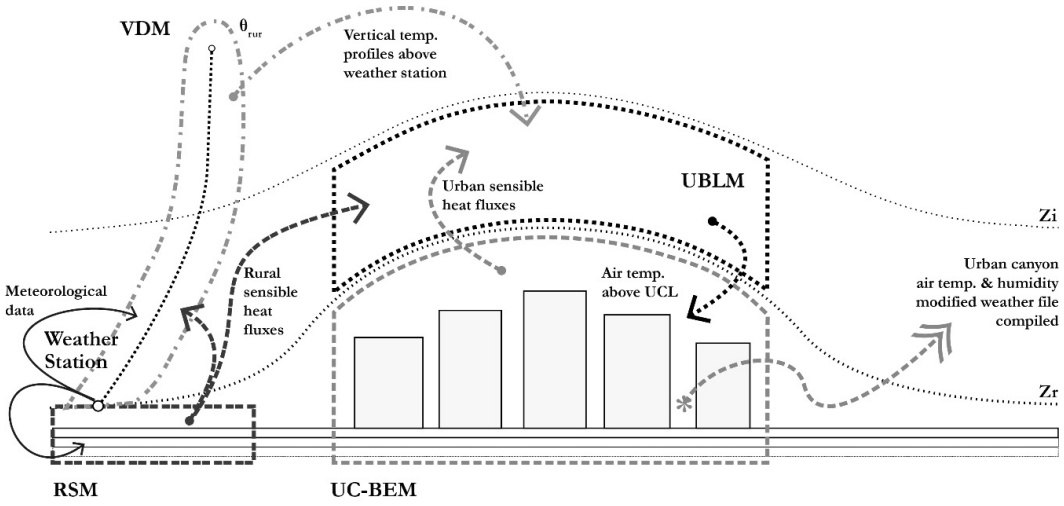

Based on: Bueno *et al.* (2013); (Gunawardena *et al.* 2017a, 2017b; Gunawardena 2015; Gunawardena & Kershaw 2017).

Figure 2. Physical domain of the UWG modules and their data exchanges for an ideal city.

As a refinement of the aforementioned BEM-TEB model introduced by Bueno *et al.* (2012a), the Urban Weather Generator (UWG) was developed to morph existing rural weather data with computed canopy layer air temperatures that account for the heat island effect at specific areas within a city (Bueno *et al.* 2013). The model is based on energy balance principles applied to urban canopy layer and boundary layer control volumes, for which boundary conditions can be imposed. The canyon morphology represents its microscale resolution, which is horizontally averaged to the neighbourhood scale to consider conditions with reasonable homogeneity. This permits the simplified assessment of neighbourhood-scale influence with relatively high computational efficiency, which is desired for real-world applicability. The latest iteration of the model (version 3.0.0) permits greater definition of different neighbourhood characteristics. This means that the energy exchanges of individual building types within the neighbourhood are simulated separately in parallel to provide better representation of real-world situations where a mix of building types is expected. The latest version also includes longwave radiation influences of urban boundary layer water vapour and carbon dioxide, as well as a revised treatment of the surface roughness influence on airflow. The latter in particular addresses a criticism of the previous version that calculated friction velocities based on empirical parameters, and now instead applies a scheme by Hanna & Britter (2002) developed explicitly for urban areas. These improvements however have had minimal consequence to the previous error margin, which remains within the range of air temperature variability (~1 K), observed in different locations within the same urban area (Bueno *et al.* 2014).

The UWG is composed of four coupled sub-models (Figure 2), including a Rural Station Model (RSM), Vertical Diffusion Model (VDM), Urban Boundary Layer Model (UBLM), and an Urban Canopy and Building Energy Model (UC-BEM); the latter based on the Masson (2000) TEB scheme and the Bueno *et al.* (2012a) building energy model. These sub-models exchange data to compute modified temperature and humidity values and compile a morphed weather file in the EnergyPlus (*epw*) format to be used by other energy simulation models. A summary of the basic data exchanges involved is presented in Table 2, while detailed descriptions are offered by Bueno *et al.* (2013, & 2014). The generator has been verified against field

data from Basel and Toulouse (maritime temperate), and Singapore (tropical rainforest), with the evaluation involving rural air temperature measurement inputs and comparison between computed and observed urban air temperatures (Bueno *et al.* 2013, 2014; Nakano *et al.* 2015). The verifications from Basel and Toulouse had demonstrated urban climate estimation to require both canopy and boundary layer effects to account for the aggregated effect of the heat island over the entire city. From the heat island effect experienced inside urban canyons, more than half is attributed to this mesoscale influence. The resolution of such boundary layer influences requires mesoscale effects to be reconciled with the aid of higher-scale atmospheric simulations coupled within a multiscale framework, which is an approach that is exemplified by the UWG framework (Bueno *et al.* 2013).

Table 2. UWG sub-model interactions.

	Rural Station Model (**RSM**)	Vertical Diffusion Model (**VDM**)	Urban Boundary Layer Model (**UBLM**)	Urban Canopy and Building Energy Model (**UC-BEM**)
Physical principle(s)	▪ Energy balance at the rural soil surface. Dividing the soil into discrete layers, the RSM solves the system of equations.	▪ Solves heat diffusion equations to determine vertical temperature profiles at the rural site.	▪ Energy balance for the control volume inside the urban boundary layer, delimited by the blending height (*Zr*) and the boundary layer height (*Zi*).	▪ Heat balance considering the heat capacity of urban canyon air. The balance accounts for heat flux from: walls, windows, road, sensible exchange between canyon air and atmosphere, heat flux from exfiltration, waste heat from anthropogenic sources, and the radiant exchange between canyon air and sky.
Reads and calculates	▪ Reads hourly values of meteorological fields measured at the rural site and calculates sensible heat flux.	▪ Reads air temperatures and velocities measured at rural weather station, and sensible heat flux inputted by the RSM, to calculate vertical profiles of air temperature above the weather station.	▪ Reads temperatures at different heights provided by the VDM and the sensible heat flux provided by the RSM and the UC-BEM to calculate air temperatures above the canopy layer (above canyons).	▪ Reads radiation, precipitation, air velocity and humidity measured at weather station, and air temperature above the canopy layer provided by the UBLM to calculate urban canyon air temperature and humidity.
Output path	▪ Sensible heat flux provided to VDM and UBL models.	▪ Vertical profiles of air temperature above weather station provided to the UBLM.	▪ Air temperatures above the canopy layer (above urban canyons) provided to UC-BEM.	▪ Urban sensible heat flux provided to UBLM; and Urban canyon air temperature and humidity modified *epw* compiled.
Assumptions	▪ Latent heat flux from vegetation evapotranspiration is calculated as a fraction (0.5 default) of the absorbed short-wave radiation. ▪ Vegetation albedo is given as 0.25 (average reported in studies). ▪ Effect of vegetation from May to November (for deciduous vegetation).		▪ Potential temperature is uniform inside the control volume. ▪ The advection problem is buoyancy-driven than forced, if circulation velocity is >air velocity at the weather station. ▪ Boundary layer is well-mixed, isothermal air below the capping inversion that is lower at night than by daytime.	▪ Air inside the canopy layer is well-mixed. ▪ Air humidity above urban canyons is the same as at the weather station for each time-step. ▪ Solar radiation received by walls and road is calculated by an average urban canyon orientation. ▪ Same RSM vegetation assumptions.

2.1.1 Limitations of the framework

Substantial computational demand has been the general criticism levelled at preceding attempts to characterise the urban climate through climatological modelling (Table 1). Addressing this had encouraged Bueno *et al.* (2013) to consider a framework approach, which was also motivated by the desire to introduce it as an adaptable tool. In keeping with this, the developers are currently reviewing sensitivity analyses to reduce the necessary fifty input parameters, data for some of which is not readily available (e.g., boundary layer data), or may have only a marginal influence on the accuracy required for practical applications. The model is also promoted as an iterative design tool that presents users with the opportunity to explore different options, rather than offering a deterministic solution (Bueno *et al.* 2014; Nakano *et al.* 2015). Such comparative assessments in turn help to nullify and limit errors arising from input assumptions.

The UWG currently presents three key limitations to consider:

- The model outputs are based on input rural weather data and morphology parameters of the site of interest. The input weather data represents the rural boundary condition, where the influence of the city is believed to be negligible. Selecting a weather station from an area where there is influence from high building density, site-specific microclimate conditions produced by surrounding orography, or the presence of large waterbodies as in coastal areas, is inappropriate and doing so is likely to lead to the generation of a modified weather file that misrepresents the studied site. In terms of outputs, it must also be emphasised that in the generation of the file only air temperatures and relative humidity are calculated, while wind velocities remain unmodified (Nakano *et al.* 2015).

- Notwithstanding the extended neighbourhood definition capabilities in the latest iteration, a significant limitation of the model remains its applicability to canyon-dominant urban morphologies. The use of the canyon is justified with reference to preceding urban modelling approaches having established it as the simplified generic representation of the urban microscale. The heterogeneity of some cities however demonstrates geometric arrangements that diverge from this ideal. The positive validation of the model reported for Europe-based cities with their relatively homogeneous morphologies is therefore not relatable for the review of sites in cities with high degrees of morphological complexity and informality. This shortcoming is acknowledged by the developers, given their own sensitivity analyses stressing critical dependence of results on input morphological parameters ('horizontal building density' and the 'vertical-to-horizontal urban area ratio'). Further development of the model is envisaged to address relatability to heterogeneous urban areas, while at present the application of the model offers best agreement for sites conforming to canyon-dominant, relatively homogeneous morphologies (Bueno *et al.* 2013, 2014).

- In addition to conserving computational efficiency, the simplified consideration of vegetation cover (latent heat flux from evapotranspiration) is justified in terms of data gathering convenience. As sophisticated vegetation models require several empirical parameters, Bueno *et al.* (2013) had argued that the inaccessibility of such detailed data regarding soil and plant composition to be a practical workflow impediment. The UWG as a result has simplified the consideration of vegetation to user-input parameters of generic coverage, latent conversion fraction for trees and grasses, participation (seasonality), and albedo; and assumes other complex vegetation parameters to have negligible influence on the expected

outcome. However, their Basel case study application (Bueno *et al.* 2013) emphasised the need to recognise better treatment of latent heat flux. Although their subsequent study of Singapore was partly introduced to address this, the topic is thinly discussed in the resulting papers, with Nakano *et al.* (2015) stressing the need for further attention in the future development of the framework. At present, the UWG could thus be expected to deliver less representative results for study sites that include or are adjacent to large coverage areas of diverse vegetation, as well as surface waterbodies.

The UWG is argued by the authors to be robust enough to generate reasonable outputs for most urban areas. The simplifications and assumptions employed to achieve a computationally efficient framework however prevents it from capturing detailed microclimate effects. As the project has focused interest in determining the significance of latent heat flux from evapotranspiration on microclimate conditions, this framework is presented here as a starting point from which a proposed improvement of latent heat flux considerations could be integrated.

3.0 Quantifying latent heat flux from evapotranspiration

The following is an overview of theory addressing the quantification of the latent heat flux from evapotranspiration. Waterbodies are considered first, followed by vegetated surfaces.

3.1 Quantifying waterbody evaporation

Evaporation from a waterbody is expressed by the rate of the volume of water that is evaporated per unit area in unit time (E_{wb}). The most direct method for measuring actual evaporation is as a residual in a water balance.

$$p_r + i + d = E_{wb} + \Delta r + \Delta S + \Delta A \qquad \textit{Equation 5}$$

$$E_{wb} = p + i + d - \Delta r - \Delta S - \Delta A$$

Where,

p_r	Precipitation [kg·m^{-2}·s^{-1}]	Δr	Net change in runoff over distance [kg·m^{-2}·s^{-1}]
i	Irrigation [kg·m^{-2}·s^{-1}]	ΔS	Net water storage [kg·m^{-2}·s^{-1}]
d	Dewfall [kg·m^{-2}·s^{-1}]	ΔA	Horizontal moisture exchange [kg·m^{-2}·s^{-1}]
E_{wb}	Evaporation from waterbody [kg·m^{-2}·s^{-1}]		

In empirical studies this rate is determined with the use of an atmometer that either measures water loss from an exposed container (evaporation pan), or from a continuously damp porous surface (Piche evaporimeter, Thom *et al.* 1981). The commonly used evaporation pan is floated on the surface of a waterbody, and accounting for rainfall and dewfall of the water balance (Equation 5), offers E_{pan} estimates typically in good agreement with estimates provided by the Penman Equation (Equation 9, discussed below) for diverse climates (Monteith & Unsworth 2013; Thom *et al.* 1981). In the deployment of the pan, care must be taken to ensure that it is not used in conditions with strong surface disturbances (i.e., waves), which could result in contamination from volume transfer. The pan used also needs to be of a material that allows for heat conduction from the waterbody to the pan water, but not itself absorb solar radiation. The inability to account for significant wave mixing, body fetch (distance measured in the upwind direction), depth, and stratification means that not all influences affecting waterbody evaporation are accounted for by this method. The heat storage influence associated with depth however can be disregarded with the use of extensive averaging periods, which for very

deep bodies is typically over a year. The Piche evaporimeter method in contrast presents E_{pi} from a continuously damp disc of absorbent paper, and is widely used owing to its calibration simplicity. As the results are dependent on wind velocity and the wet-bulb saturation deficit, it is used within a sheltered meteorological screen. The measurements obtained provide a representation of the drying power of the atmosphere and its aerodynamic resistance to vapour transport, which is proportional to the advection term in the Penman Equation (Equation 8, discussed below), with studies highlighting good agreement with long-term values for this term (Papaioannou *et al.* 1996). A number of methodologies have also been presented to relate E_{pi} measurements to the evaporation estimated by the Penman Equation (E_{Pen}) (e.g., Stanhill 1962; Thom *et al.* 1981), which negates the need for using complex instrumentation to determine evaporation. Given the limitations highlighted, atmometer readings from both methods are unlikely to precisely compare to actual evaporation from natural bodies. They are thus mostly of use for benchmarking and comparative analyses in similar climates (Sartori 2000).

Theoretical models that quantify evaporation acknowledge its dependence on the availability of water (i.e., abundance of the fluid), availability of energy to enable phase change, the existence of a vapour gradient, and a turbulent atmosphere to advect away vapour. The climate parameters relevant for these dependencies are air and water temperature, pressure, wind velocity, and relative humidity. There are many formulations in the literature for calculating the evaporation rate derived from these parameters, the vast majority of which are based on empirical evaporative heat transfer coefficients. The application of such empirical equations must thus correspond to the conditions of original studies, as their coefficients are derived from specific correlations of psychrometric parameters (Sartori 2000).

A universal model for describing evaporation is partly derived from an energy balance approach, which accounts for the energy available for phase change. For a given waterbody, this balance may be expressed as follows:

$$Q^* = Q_{E_{wb}} + Q_H + Q_G + Q_R + \Delta Q_S + \Delta Q_A \qquad \textit{Equation 6}$$

$$Q_{E_{wb}} = Q^*_{wb} - Q_H - Q_G - Q_R - \Delta Q_S - \Delta Q_A$$

$$E_{wb} = Q_{E_{wb}}/\lambda \qquad \textit{Equation 7}$$

Where,

ΔQ_A	Net horizontal heat advection due to water currents [W·m^{-2}]
ΔQ_s	Change in heat storage [W·m^{-2}]
E_{wb}	Rate of loss of water per unit surface area in time from waterbody [kg·m^{-2}·s^{-1}]
Q_G	Heat conduction into or out of the underlying soil [W·m^{-2}]
Q^*_{wb}	Net all-wave radiation available [W·m^{-2}]
Q_R	Net heat transfer by rainfall [W·m^{-2}]
λ	Latent heat of water ~2.43 MJ·kg^{-1}

The vapour generated with the aid of this energy is then vacated to sustain evaporation, as it is with all natural open-system evaporation processes. To reflect this Penman (1948) combined the availability of energy considered above (energy term), with the drying power of the atmosphere and its aerodynamic resistance to transport (advection or vapour deficit term), to present his 'Combination Model'. The evaporation rate (E_{Pen}) from a water surface exposed to atmosphere that is partially saturated is expressed in the common form of the equation as follows:

$$\lambda E_{Pen} = \frac{m\,Q^*_{wb}}{m+\gamma^*} + \frac{\rho c_p \{e_s(T)-e\}\, r_H^{-1}}{m+\gamma^*}. \qquad \textit{Equation 8}$$

Energy Term ***Advection/ vapour deficit Term***

$$E_{Pen} = \frac{m\,Q^*_{wb} + \rho c_p \{e_s(T)-e\}\, r_H^{-1}}{\lambda\,(m+\gamma^*)}. \qquad \textit{Equation 9}$$

Where,

E_{Pen}	Rate of loss of water per unit area from Penman Equation [kg·m^{-2}·s^{-1}]
Q^*_{wb}	Net radiation received by waterbody [W·m^{-2}]
c_p	Specific heat of air at constant pressure [J·kg^{-1}·K^{-1}]
$e_s(T)$	Saturation vapour pressure of water vapour at temperature T [Pa]
r_H	Resistance for sensible heat transfer [s·m^{-1}]
r_V	Resistance for water vapour transfer [s·m^{-1}]
γ^*	Apparent value of psychrometric constant = $\gamma\, r_V/r_H$ [Pa·K^{-1}]
e	Partial pressure of water vapour in air [Pa]
m	Rate of change of saturation vapour pressure with temperature = $\delta e_s(T)/\delta T$ [Pa·K^{-1}]
γ	Psychrometric constant ($c_p\rho/\lambda\epsilon$) ~66 Pa·K^{-1}
λ	Latent heat of water ~2.43 MJ·kg^{-1}
ρ	Density of air [kg·m^{-3}]
ϵ	Ratio of molecular weights of water vapour and air (0.622) [-]

3.2 Quantifying vegetation evapotranspiration

The direct method for measuring actual transpiration (E_{veg}) is achieved as a residual in a water balance calculation.

$$p_r + i + d = E_{veg} + \Delta r + \Delta S + \Delta A \qquad \textit{Equation 10}$$

$$E_{veg} = p + i + d - \Delta r - \Delta S - \Delta A$$

Where,

p_r	Precipitation [kg·m^{-2}·s^{-1}]	Δr	Net change in runoff over distance [kg·m^{-2}·s^{-1}]
i	Irrigation [kg·m^{-2}·s^{-1}]	ΔS	Net water storage [kg·m^{-2}·s^{-1}]
d	Dewfall [kg·m^{-2}·s^{-1}]	ΔA	Horizontal moisture exchange [kg·m^{-2}·s^{-1}]
E_{veg}	Transpiration from vegetation [kg·m^{-2}·s^{-1}]		

With empirical approaches for quantifying the evapotranspiration from larger areas of vegetation climatologists commonly use the eddy correlation method, which involves the measurement of vertical velocity and relative humidity of air flow above the area of interest to calculate the upward flux of vapour (Oke 1987). An alternative approach to this involves sample surveys and experiments of representative areas that can be scaled-up to present generalised findings for larger areas. For smaller plants, this can be achieved by measuring their weight and calculated from a mass balance. For larger plants, stomatal resistance may be measured using a porometer or infrared gas analyser (IRGA) applied to their leaves, and with the additional measurement of leaf and air temperature, atmospheric pressure, relative humidity, and leaf area of the tree, an instantaneous rate of water loss can be quantified. Sap-flow meters commonly used in cultivated groves may also be used to calculate volume flow of water up vegetation trunks (Ennos & Percival 2011). Scaling-up such findings to larger areas however can be problematic in urban areas where heterogeneity of plants is expected and encouraged for other ecological benefits. Even with similar vegetation types, it has been found that there are large

differences in water loss between those growing over grass as opposed to asphalt (Kjelgren & Montague 1998). It is therefore difficult to determine 'typical values' of transpiration that can be readily applied to urban areas (Ennos & Percival 2011). Furthermore, there is considerable resource expense (time, labour, and apparatus), and longitudinal monitoring difficulties to address with all empirical approaches listed above.

3.2.1 Growth and transpiration

Researchers have attempted to determine transpiration rates with reference to growth and carbon sequestration. This is based on the principle that transpiration water loss occurs when stomata are opened to achieve photosynthesis (Equation 11), the rate of transpiration should be directly proportional to the photosynthetic rate of the vegetation (Ennos & Percival 2011).

Photosynthesis:

$$6\,CO_2 + 6\,H_2O + Q_{rad}\,(solar\ radiation) = C_6H_{12}O_6\,(Glucose) + 6\,O_2 \quad \textit{Equation 11}$$

Respiration:

$$C_6H_{12}O_6 + 6\,O_2 = 6\,CO_2 + 6\,H_2O + Q_{res}\,(combustion) \quad \textit{Equation 12}$$

Vegetation growth is quantified by the dry matter gained from photosynthesis. The sequestration of CO_2 by gross photosynthesis (converting inorganic carbon to organic compounds, Equation 11), minus its rejection from respiration (Equation 12), presents the net rate of photosynthesis (ΔP), which is equivalent to growth. Measuring the rate of photosynthesis enables the water use efficiency of photosynthesis to be determined. Farquhar *et al.* (1980) for example calculated that for every mole of water lost, between 2×10^{-3} and 4×10^{-3} moles of CO_2 are sequestrated. This water use efficiency of conventionally photosynthesising C3 plants is consistent and thus applicable to most tree species. Measuring photosynthesis however is a challenging task, while measuring tree growth and estimating the rate of sequestration of biomass are typically within the capabilities of arborists. Empirical studies have shown that 50% of photosynthesis is typically converted into biomass production, which translates to water loss per unit of aboveground biomass sequestration of trees to between 0.4 and 0.66 tonnes of water per kilogram of biomass sequestered (Ennos & Percival 2011). When the latent heat of water (λ) is accounted, this would present a cooling range $Q_{E_{veg}}$ expected for a given tree. This approach highlights that the cooling potential of trees could be increased by enhancing their growth, subject to sufficient availability of water supply. This is often used to justify planting fast growing, yet water-demanding trees in Mediterranean urban areas, as opposed to the expected approach of planting drought-tolerant trees.

3.2.2 Simulation models

The latent heat flux $Q_{E_{veg}}$ for a given vegetated surface can be derived from its energy balance as a residual if all other components are known or solved. The energy that is locked in as the net rate of biochemical energy storage (ΔQ_P), is negligible in comparison to other terms of a vegetated system and thus is typically disregarded in calculations (Oke 1987).

$$Q^*_{veg} = Q_{E_{veg}} + Q_H + Q_{G_{veg}} + \Delta Q_P + \Delta Q_S + \Delta Q_A \quad \textit{Equation 13}$$

$$Q_{E_{veg}} = Q^*_{veg} - Q_H - Q_{G_{veg}} - \Delta Q_P - \Delta Q_S - \Delta Q_A$$

Where,

Q^*_{veg}	Net all-wave radiation received by vegetation [W·m^{-2}]
$Q_{G_{veg}}$	Heat conduction into or out of the underlying soil [W·m^{-2}]
ΔQ_P	Net rate of biochemical energy storage due to photosynthesis [W·m^{-2}]
ΔQ_S	Net rate of physical heat storage by substances [W·m^{-2}]
ΔQ_A	Net energy due to horizontal sensible and latent heat transport [W·m^{-2}]

Considering a vegetated area as a volumetric system means that it does not account for the internal exchanges between individual plants. The approach is therefore a simplification that enables a reasonable estimate to be obtained for a relatively homogenous (type and age) vegetated 'community', such as a crop or grove (Oke 1987). The contrary however is common in most vegetated urban areas, where even isolated trees may be significant. Considering the energy balance for an isolated tree (Figure 3), suggests that its heat flux is likely to be greater than would be for urban grasslands, groves, or forests. This enhanced per unit benefit is attributed to its opportunity to capture greater solar radiation, grow faster, and cast shade over greater ground area than canopy trees. Notwithstanding this identified significance, transpiration studies have typically preferred to consider homogenous vegetated communities from the simplest representation of a short crop to more complex forests and groves, principally in the interest of presenting generalisable findings. The assessment and discussion of individual trees is therefore underrepresented in the available literature (Gunawardena *et al.* 2017c).

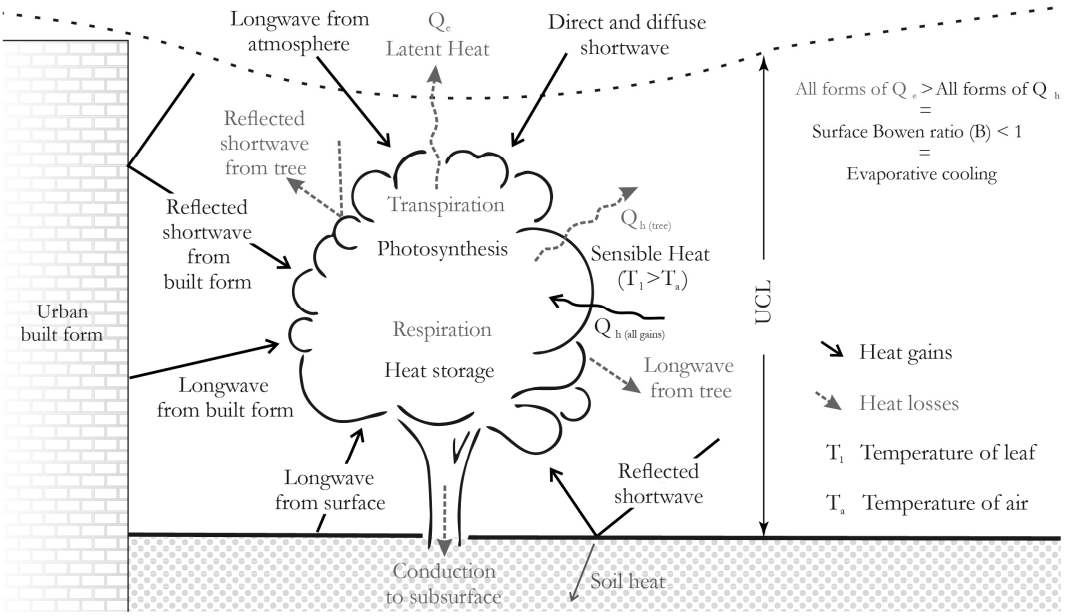

Figure 3. Daytime energy exchanges between a tree and the surrounding built environment.

Penman (1948) advanced his model for calculating evaporation from a water surface (Equation 9), to consider the transpiration expected from the simplest representation of a homogenous vegetated surface, which he defined as a well-watered short green crop that completely shaded the ground. With the assumption that the turbulent flow above this crop was parametrised in the aerodynamic term of the equation, he calculated the transpiration from this hypothetical crop with only the incorporation of the estimated net radiation received (Monteith & Unsworth 2013). The resulting value was described as the 'potential evaporation' (Penman

1948), which is commonly referred to by agronomists as the 'reference evaporation' (ET_0). The resulting calculations using various forms of the original Penman Equation have been found by empirical observations to offer transpiration estimates in good agreement with well-watered short crops in temperate regions (Monteith & Unsworth 2013). Agronomists of the present-day however use the advanced Penman-Monteith form of the equation (discussed below), to estimate ET_0 for a hypothetical crop with rigidly defined characteristics (Allen *et al.* 1998). The only factors affecting this ET_0 are climate parameters that can be calculated from weather data, with evaporating influence of the atmosphere at any location and time estimated without reference to crop characteristics and soil influences. By incorporating crop factors (K_c) that address crop characteristics and growth stage (Equation 14), transpiration for a range of well-watered crops can be estimated (Monteith & Unsworth 2013). Furthermore, to calculate transpiration from drought stressed crops, K_c can be modified by incorporating an additional stress factor (K_s) proportional to the matric potential of the soil (Allen *et al.* 1998). Although such crop factors are available for many crop types, there is limited data currently available for urban vegetation types (Ennos & Percival 2011).

$$E_{crop} = ET_0 + K_c \qquad \textit{Equation 14}$$

When considering vegetated systems with limited water availability, less complete ground cover, and complex canopies, the abovementioned Penman-Monteith Equation provides better representation of transpiration rates (E_{PenM}) as it accounts for stomatal resistance (r_s) to water loss. This equation only defers from the Penman Equation (Equation 9), by the inclusion of the resistance specifying evaporation limits imposed by leaf stomata to the psychrometric constant (γ) term (Monteith & Unsworth 2013). The equation for an amphistomatous leaf (stomata on both sides) is presented as follows:

$$\lambda E_{PenM} = \frac{m\, Q^*_{veg}}{[m+\gamma\,(1+r_s/r_H)]} + \frac{\rho c_p \{e_s(T)-e\}\, r_H^{-1}}{[m+\gamma\,(1+r_s/r_H)]}. \qquad \textit{Equation 15}$$

$$\lambda E_{PenM} = \frac{m\, Q^*_{veg} + \rho c_p \{e_s(T)-e\}\, r_H^{-1}}{(m+\gamma)\,(1+r_s/r_H)}. \qquad \textit{Equation 16}$$

Where,

r_s	Resistance of a set of stomata [s·m^{-1}]

This Penman-Monteith Equation can be applied to a single leaf as well as to a uniform canopy of vegetation. When applying to a canopy, the stand-atmosphere exchange is expressed in terms of an aerodynamic resistance (r_a) corresponding to the boundary layer resistance (r_H) around a leaf, and a canopy resistance (r_c) that corresponds to the stomatal resistance (r_s) of a leaf (Monteith & Unsworth 2013). When considering such large canopy areas, it is also necessary to include the conduction of heat into the soil and biomass ($Q_{G_{veg}}$) in the energy balance (Monteith & Unsworth 2013). The canopy scale form of the Penman-Monteith Equation is therefore represented as follows:

$$\lambda E_{PenM} = \frac{m\left(Q^*_{veg} - Q_{G_{veg}}\right) + \rho c_p \{e_s(T)-e\}\, r_a^{-1}}{(m+\gamma)(1+r_c/r_a)}. \qquad \textit{Equation 17}$$

The Penman-Monteith Equation may be simplified when the boundary layer resistance (r_H) that connects a leaf to its surrounding atmosphere (or the equivalent r_a for an extensive canopy area) becomes either very large or non-existent. When it becomes very large, the leaf is weakly

coupled to the bulk flow of the surrounding atmosphere, and the advection term collapses to only leave the energy term (Equation 18); a state that is described as the 'equilibrium evaporation' (λE_{eq}). As the boundary layer resistance is substantially reduced, the leaf becomes strongly coupled to the bulk flow of the surrounding atmosphere, and the energy term collapses to leave the advection term as expressed in Equation 19. Jarvis & McNaughton (1986) defined this as the 'imposed evaporation' (λE_i).

$$\lambda E_{PenM} = \frac{m Q^*_{veg}}{[m + \gamma (1 + r_s/r_H)]} = \lambda E_{eq} \qquad \textit{Equation 18}$$

$$\lambda E_{PenM} = \frac{\rho c_p \{e_s(T) - e\} r_H^{-1}}{[m + \gamma (1 + r_s/r_H)]} = \frac{\rho c_p \{e_s(T) - e\}}{[m r_H + \gamma (r_H + r_s)]} = \lambda E_i \qquad \textit{Equation 19}$$

A leaf, canopy, or landscape transpiration is said to be between the two limits of λE_{eq} and λE_i, with the relationship to general evaporation (λE) presented by Jarvis & McNaughton (1986) as follows:

$$\lambda E = \Omega \lambda E_{eq} + (1 - \Omega) \lambda E_i, \qquad \textit{Equation 20}$$

Where,

Ω Decoupling coefficient defined for well-watered vegetation [-]

As the decoupling coefficient describes the relationship between vegetation foliage and the bulk flow of the atmosphere, for individual leaves it depends principally on wind velocity and leaf area, while when considering larger canopy areas it is dependent mainly on wind velocity and surface roughness. In the case of smaller leaves that are typically well coupled to the bulk flow of the atmosphere, an increase in stomatal resistance is likely to result in a proportional decrease in transpiration. The stomata of smaller leaves can therefore exert greater control over their water loss rates (Monteith & Unsworth 2013). With larger leaves that are weakly coupled to the bulk flow of the atmosphere, transpiration is less controlled by stomata and is more dependent on radiant energy availability. When considering larger canopy areas of vegetation, the smoother surfaces with large aerodynamic resistances (e.g., short grasses) are weakly coupled to the bulk flow, which results in their transpiration rates being largely controlled by the available energy, and is unaffected by the canopy (stomatal) resistance and saturation deficit (advection term). This explains why the Penman Equation (Equation 9) is generally effective in estimating water loss from well-watered short grasses. Transpiration from coarser canopies with low aerodynamic resistances and better coupled to the bulk flow of the atmosphere are instead controlled by the changes in canopy resistance and are dependent on the advective term (Monteith & Unsworth 2013; Oke 1987). This in turn emphasises the significance of determining the roughness or aerodynamic resistances provided by vegetation canopies when quantifying the transpiration expected from such surfaces.

4.0 Summary

The above review discussed methodologies for assessing urban microclimates, ranging from historical data-based models to complex frameworks involving a range of individual approaches associated in one-way, two-way, or multiple data exchanges. With multiscale coupling, the sub-models remain discrete in a framework that favours multiple approaches such

as empirical, analytical, or numerical methods to be utilised to solve problems relating to discrete spatial and temporal scales. This approach also favours the subsequent coupling of submodels that specifically target the resolution of a set of problems to be incorporated into the framework in a computationally efficient manner. The review of the recently developed exemplar UWG microclimate framework highlighted that although most aspects of the urban energy balance were reasonably addressed, the latent heat flux from evapotranspiration had been considerably simplified. As this project has interest in determining the significance of this flux, the UWG framework presents potential for further improvement. The above as a result also reviewed principal approaches available for determining this latent heat flux, including variations of the Penman-Monteith model to highlight potential for its coupling to be considered in the future development of the framework.

Acknowledgements

This work was funded by UKRI, Engineering and Physical Sciences Research Council grant [1930753]. For the purpose of open access, the author has applied a Creative Commons Attribution (CC BY) licence to any Author Accepted Manuscript version arising.

Bibliography

Allen, R. G., Pereira, L. S., Raes, D., & Smith, M. (1998). Crop evapotranspiration-Guidelines for computing crop water requirements-FAO Irrigation and drainage paper 56. *FAO, Rome*, **300**(9), D05109.

Bruse, M. (2004). *ENVI-met implementation of the Jacobs A− gs Model to calculate the stomata conductance*, Bochum.

Bueno, B., Norford, L., Hidalgo, J., & Pigeon, G. (2013). The urban weather generator. *Journal of Building Performance Simulation*, **6**(4), 269–281.

Bueno, B., Norford, L., Pigeon, G., & Britter, R. (2011). Combining a Detailed Building Energy Model with a Physically-Based Urban Canopy Model. *Boundary-Layer Meteorology*, **140**(3), 471–489.

Bueno, B., Norford, L., Pigeon, G., & Britter, R. (2012a). A resistance-capacitance network model for the analysis of the interactions between the energy performance of buildings and the urban climate. *Building and Environment*, **54**, 116–125.

Bueno, B., Pigeon, G., Norford, L. K., Zibouche, K., & Marchadier, C. (2012b). Development and evaluation of a building energy model integrated in the TEB scheme. *Geoscientific Model Development*, **5**(2), 433–448.

Bueno, B., Roth, M., Norford, L., & Li, R. (2014). Computationally efficient prediction of canopy level urban air temperature at the neighbourhood scale. *Urban Climate*, **9**, 35–53.

Chung, T. J. (2002). *Computational fluid dynamics*, Cambridge: Cambridge University Press.

Crawley, D. B. (2007). Estimating the impacts of climate change and urbanization on building performance. *Journal of Building Performance Simulation*, **1**(2), 91–115.

Crawley, D. B., Lawrie, L. K., Winkelmann, F. C., … Glazer, J. (2001). EnergyPlus: creating a new-generation building energy simulation program. *Energy and Buildings*, **33**(4), 319–331.

Ennos, R., & Percival, G. (2011). Quantifying the cooling benefits of urban trees. In *Trees, people and the built environment*, Birmingham: Forestry Commission, pp. 113–118.

Erell, E., & Williamson, T. (2006). Simulating air temperature in an urban street canyon in all weather conditions using measured data at a reference meteorological station. *International Journal of Climatology*, **26**(12), 1671–1694.

Farquhar, G. D., Caemmerer, S. von, & Berry, J. A. (1980). A biochemical model of photosynthetic CO2 assimilation in leaves of C3 species. *Planta*, **149**(1), 78–90.

Grimmond, C. S. B., Blackett, M., Best, M. J., … Zhang, N. (2010a). The International Urban Energy Balance Models Comparison Project: First Results from Phase 1. *Journal of Applied Meteorology and Climatology*, **49**(6), 1268–1292.

Grimmond, C. S. B., Cleugh, H. A., & Oke, T. R. (1991). An objective urban heat storage model and its comparison with other schemes. *Atmospheric Environment. Part B. Urban Atmosphere*, **25**(3), 311–326.

Grimmond, C. S. B., & Oke, T. R. (2002). Turbulent heat fluxes in urban areas: Observations and a local-scale urban meteorological parameterization scheme (LUMPS). *Journal of Applied Meteorology*, **41**(7), 792–810.

Grimmond, C. S. B., Roth, M., Oke, T. R., … Emmanuel, R. (2010b). Climate and more sustainable cities: climate information for improved planning and management of cities (producers/capabilities perspective). *Procedia Environmental Sciences*, **1**, 247–274.

Gunawardena, K. (2018). *Fundamentals of Urban Heat Islands: Concise guide for architects and urban planners [Ph.D Paper]*, University of Cambridge, Cambridge.

Gunawardena, K., Kershaw, T., & McCullen, N. (2017a). The influence of urban climate on building energy use. In *8th International Conference on Structural Engineering and Construction Management*, Kandy: ICSECM.

Gunawardena, K. R. (2015). *Residential overheating risk in an urban climate [M. Phil Thesis]*, University of Cambridge, Cambridge.

Gunawardena, K. R. (2021). *Vertical greening in urban built environments [Ph.D Thesis]*, University of Cambridge. Retrieved from https://doi.org/10.17863/CAM.82336

Gunawardena, K. R., & Kershaw, T. (2017). Urban climate influence on building energy use. In M. P. Burlando, Massimiliano; Canepa, Maria; Magliocco, Adriano; Perini, Katia, Repetto, ed., *International Conference on Urban Comfort and Environmental Quality URBAN-CEQ*, Genoa: Genoa University Press, pp. 175–184.

Gunawardena, K. R., Mccullen, N., & Kershaw, T. (2017b). Heat island influence on space-conditioning loads of urban and suburban office buildings. In *Cities and Climate Conference 2017*, Potsdam: Potsdam Institute for Climate Impact Research, pp. 1–13.

Gunawardena, K. R., Wells, M. J., & Kershaw, T. (2017c). Utilising green and bluespace to mitigate urban heat island intensity. *Science of the Total Environment*, **584**–**585**, 1040–1055.

Hanna, S. R., & Britter, R. E. (2002). *Wind flow and vapor cloud dispersion at industrial and urban sites*, Vol. 7, New York: John Wiley & Sons.

Hidalgo, J., Pigeon, G., & Masson, V. (2008). Urban-breeze circulation during the CAPITOUL experiment: observational data analysis approach. *Meteorology and Atmospheric Physics*, **102**(3–4), 223–241.

Jacobson, M. Z. (2005). *Fundamentals of atmospheric modeling*, Cambridge: Cambridge University Press.

Jarvis, P. G., & McNaughton, K. G. (1986). Stomatal control of transpiration: scaling up from leaf to region. *Advances in Ecological Research*, **15**, 1–49.

Kikegawa, Y., Genchi, Y., Yoshikado, H., & Kondo, H. (2003). Development of a numerical simulation system toward comprehensive assessments of urban warming countermeasures including their impacts upon the urban buildings' energy-demands. *Applied Energy*, **76**(4), 449–466.

Kim, Y.-H., & Baik, J.-J. (2002). Maximum Urban Heat Island Intensity in Seoul. *Journal of Applied Meteorology*, **41**(6), 651–659.

Kjelgren, R., & Montague, T. (1998). Urban tree transpiration over turf and asphalt surfaces. *Atmospheric Environment*, **32**(1), 35–41.

Kolokotroni, M., Davies, M., Croxford, B., Bhuiyan, S., & Mavrogianni, A. (2010). A validated methodology for the prediction of heating and cooling energy demand for buildings within the Urban Heat Island: Case-study of London. *Solar Energy*, **84**(12), 2246–2255.

Kolokotroni, M., & Giridharan, R. (2008). Urban heat island intensity in London: An investigation of the impact of physical characteristics on changes in outdoor air temperature during summer. *Solar Energy*, **82**(11), 986–998.

Kolokotroni, M., Zhang, Y., & Giridharan, R. (2009). Heating and cooling degree day prediction within the London urban heat island area. *Building Services Engineering Research and Technology*, **30**(3), 183–202.

Kolokotroni, M., Zhang, Y. P., & Watkins, R. (2007). The London Heat Island and building cooling design. *Solar Energy*, **81**(1), 102–110.

Kondo, H., & Kikegawa, Y. (2003). Temperature variation in the urban canopy with anthropogenic energy use. *Pure and Applied Geophysics*, **160**(1–2), 317–324.

Martilli, A., Clappier, A., & Rotach, M. W. (2002). An urban surface exchange parameterisation for mesoscale models. *Boundary-Layer Meteorology*, **104**(2), 261–304.

Masson, V. (2000). A physically-based scheme for the urban energy budget in atmospheric models. *Boundary-Layer Meteorology*, **94**(3), 357–397.

Monteith, J., & Unsworth, M. (2013). *Principles of environmental physics*, 4th edn, Oxford: Academic Press, an imprint of Elsevier.

Nakano, A., Bueno, B., Norford, L., & Reinhart, C. F. (2015). Urban Weather Generator - A novel workflow for integrating urban heat island effect within urban design process. *Building Simulation 2015*, Hyderabad, India: International Building Performance Simulation Association.

Oke, T. R. (1981). Canyon Geometry and the Nocturnal Urban Heat-Island - Comparison of Scale Model and Field Observations. *Journal of Climatology*, **1**(3), 237-.

Oke, T. R. (1982). The Energetic Basis of the Urban Heat-Island. *Quarterly Journal of the Royal Meteorological Society*, **108**(455), 1–24.

Oke, T. R. (1987). *Boundary Layer Climates*, 2nd edn, London: Methuen.

Oxizidis, S., Dudek, A. V, & Papadopoulos, A. M. (2008). A computational method to assess the impact of urban climate on buildings using modeled climatic data. *Energy and Buildings*, **40**(3), 215–223.

Papaioannou, G., Vouraki, K., & Kerkides, P. (1996). Piche evaporimeter data as a substitute for Penman equation's aerodynamic term. *Agricultural and Forest Meteorology*, **82**(1), 83–92.

Penman, H. L. (1948). Natural evaporation from open water, bare soil and grass. *Proceedings of the Royal Society of London A: Mathematical, Physical and Engineering Sciences*, The Royal Society, pp. 120–145.

Pigeon, G., Lemonsu, A., Long, N., Barrié, J., Masson, V., & Durand, P. (2006). Urban thermodynamic island in a coastal city analysed from an optimized surface network. *Boundary-Layer Meteorology*, **120**(2), 315–351.

Pigeon, G., Zibouche, K., Bueno, B., Le Bras, J., & Masson, V. (2014). Improving the capabilities of the Town Energy Balance model with up-to-date building energy simulation algorithms: an application to a set of representative buildings in Paris. *Energy and Buildings*, **76**, 1–14.

Sailor, D. J. (2011). A review of methods for estimating anthropogenic heat and moisture emissions in the urban environment. *International Journal of Climatology*, **31**(2), 189–199.

Sartori, E. (2000). A critical review on equations employed for the calculation of the evaporation rate from free water surfaces. *Solar Energy*, **68**(1), 77–89.

Stanhill, G. (1962). The use of the Piche evaporimeter in the calculation of evaporation. *Quarterly Journal of the Royal Meteorological Society*, **88**(375), 80–82.

Swaid, H., & Hoffman, M. E. (1990). Prediction of Urban Air-Temperature Variations Using the Analytical CTTC Model. *Energy and Buildings*, **14**(4), 313–324.

Thom, A. S., Thony, J. -L L., & Vauclin, M. (1981). On the proper employment of evaporation pans and atmometers in estimating potential transpiration. *Quarterly Journal of the Royal Meteorological Society*, **107**(453), 711–736.

Yang, X. S., Zhao, L. H., Bruse, M., & Meng, Q. L. (2013). Evaluation of a microclimate model for predicting the thermal behavior of different ground surfaces. *Building and Environment*, **60**, 93–104.